Research on Heliostat Field Optimization Based on Monte Carlo Theorem and Randomized Algorithms

Yanqi Gao [1, #, *], Ziqi Yang [2, #], Zixiong Yang [2, #]

[1] Department of Automation, Beijing University of Technology, Beijing, China, 100124

[2] Department of Computer, Beijing University of Technology, Beijing, China, 100124

* Corresponding Author Email: catherine_guyu@163.com

[#]These authors contributed equally.

Abstract. The text discusses a mathematical model established for calculating the optical efficiency of heliostat fields in solar power systems. It's grounded in geometric optics algorithms and considers factors affecting the field's optical efficiency. Each heliostat and the ground have independent coordinate systems for assessing whether light is blocked. The Monte Carlo method is utilized to determine the proportion of blocked light in reflected rays. This approach accommodates the conical nature of solar radiation, enhancing accuracy by transitioning from parallel to conical light representation. The results indicate an annual average optical efficiency of 0.5084 for the heliostat field, an annual average thermal power output of 30.879 MW, and 0.4915 kW/m^2 as the annual average thermal power output per unit mirror area.

Keywords: Geometric Optics, Heliostat Field Efficiency Model, Intelligent Optimization Algorithms, Conical Light Beam, Ray Tracing Method.

1. Introduction

In China's development of a new energy-centered power system, tower-type solar thermal power generation stands out as a sustainable, low-carbon clean energy technology. It harnesses sunlight using heliostats, which focus solar energy onto a receiver, converting it into thermal energy and subsequently electricity. One of the key challenges in the construction of tower solar thermal power plants is the optimization of the heliostat field layout. This study focuses on employing optimization algorithms to improve the calculation of optical efficiencies, particularly addressing issues like shadowing and blocking within the heliostat field. Optimizing these aspects is crucial for enhancing the overall efficiency of the power generation process.

2. The research process and method

2.1. Optical Efficiency

The optical efficiency η of the heliostat is defined as

$$\eta = \eta_{sb}\eta_{cos}\eta_{at}\eta_{trunc}\eta_{ref} \tag{1}$$

where η_{sb} represents the shadow-blocking efficiency, η_{cos} is the cosine efficiency, η_{at} is the atmospheric transmittance, η_{trunc} is the receiver truncation efficiency, and η_{ref} is the reflectivity of the mirror surface. Therefore, knowing the shadow-blocking and cosine efficiencies of the heliostat allows for the calculation of optical efficiency. Additionally, the truncation efficiency can be derived from the known average thermal power output per unit mirror area.

The shadow-blocking efficiency η_{sb} is defined as:

$$\eta_{sb} = 1 - \xi \tag{2}$$

The shadow-blocking efficiency η_{sb} includes the shadow-blocking loss ξ, which can be generally divided into three parts: first, the shadow loss caused by the tower to the heliostat field, where the

sunlight is blocked by the tower and cannot directly illuminate the field. Second, the shadow loss for the rear heliostats, which occurs when the sunlight received by them is obstructed by the front heliostats. Third, the blockage loss for the rear heliostats, occurring when they reflect sunlight but are obstructed by the front heliostats.

2.2. Coordinate System

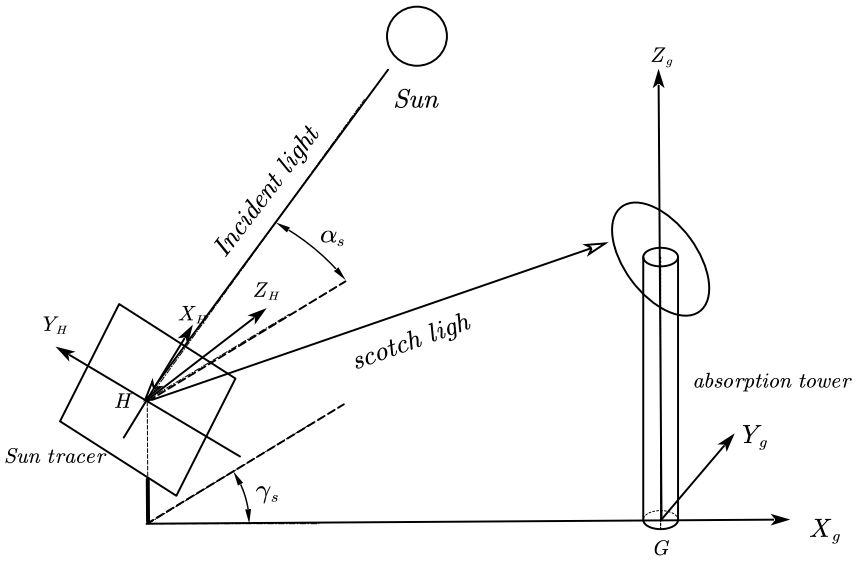

Figure 1. Mirror Coordinate System and Ground Coordinate System

As illustrated in Figure 1, a ground coordinate system $X_gY_gZ_g$ is established with G as the origin. Here, the X_g axis points horizontally towards true south, the Y_g axis horizontally towards true east, and the Z_g axis vertically upwards, perpendicular to the ground. Additionally, a mirror coordinate system $X_HY_HZ_H$ is established with H as the origin. In this system, the X_H axis coincides with the horizontal axis of the heliostat, the Y_H axis is vertically upwards, perpendicular to the Y_H axis, and the $Z_H$axis aligns with and points in the direction of the heliostat's center normal. The solar altitude angle and solar azimuth angle are denoted by α_s and γ_s, respectively.

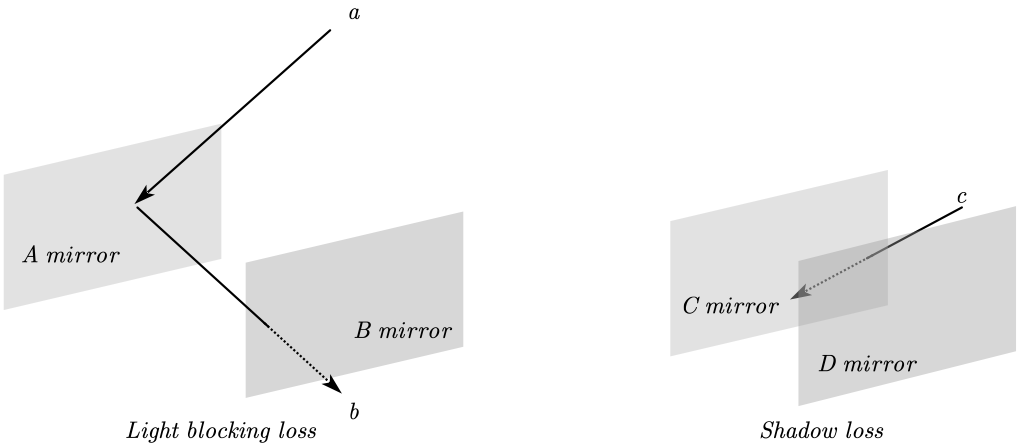

Figure 2. Simulation of Blockage Effect

As depicted in Figure 2, the incident light rays, labeled as 'a' and 'c', and their interactions with mirrors A, B, C, and D are shown. Ray 'a' is incident on mirror A and is intended to reflect towards the absorber tower, but it is blocked by mirror B, resulting in blockage loss. Similarly, when mirror C is positioned to receive the incident ray 'c', it is obstructed by mirror D, causing a shadow on mirror C and leading to shadow loss. This figure illustrates the complex interactions of light and mirrors in a heliostat field, highlighting the importance of strategic mirror placement to minimize losses [1].

2.3. Monte Carlo algorithm

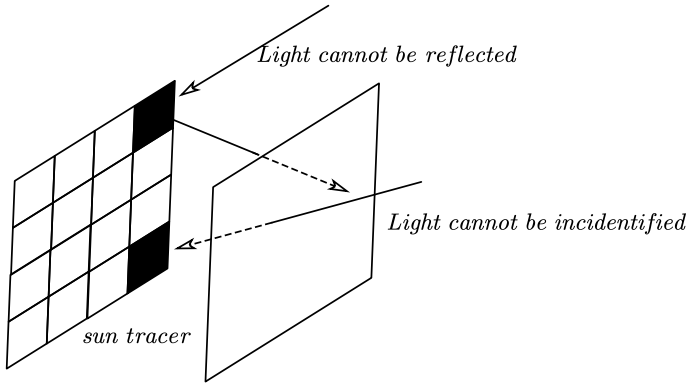

Figure 3. Schematic Diagram of Abnormal Reflection of Light Rays

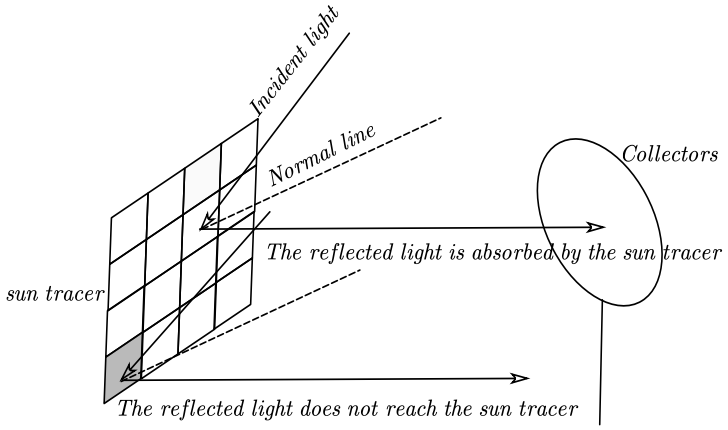

Figure 4. Schematic Diagram of Normal Reflection of Light Rays

As demonstrated in Figures 3 and 4, the heliostat is divided into 'n' smaller sections. The effectiveness of each section is determined by assessing whether the reflected rays intersect the plane of the receiver, categorizing them as either effective or ineffective. The obstruction efficiency is then calculated as the ratio of effective sections to the total number of sections. This method allows for a detailed analysis of the heliostat's performance, taking into account the complex interplay of light, reflection, and geometry in the system.

2.4. Conical Light Column

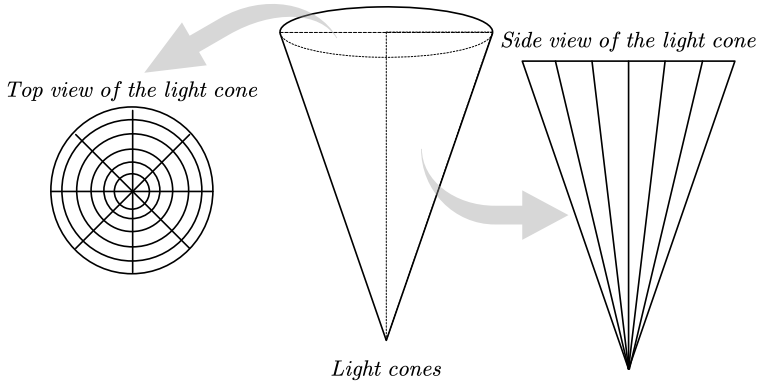

Figure 5. Schematic Diagram of the Equiangular Method

Within the sun divergence Angle, several incident rays are tracked in a uniform step size division, as shown in Figure 5. This method involves evenly dividing steps in both the semi-angle widening direction and the circumferential direction. To solve the expression of a particular ray within the light cone, the study establishes a light cone coordinate system as shown in Figure 6:

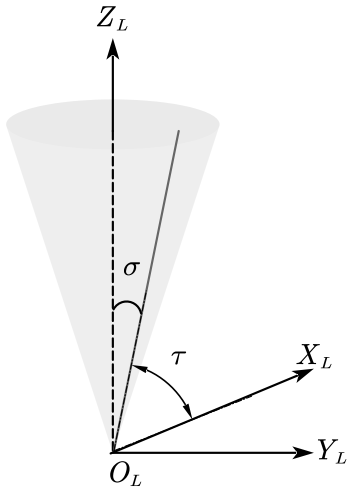

Figure 6. Schematic Diagram of the Light Cone Coordinate System

2.5. Ray Tracing Method

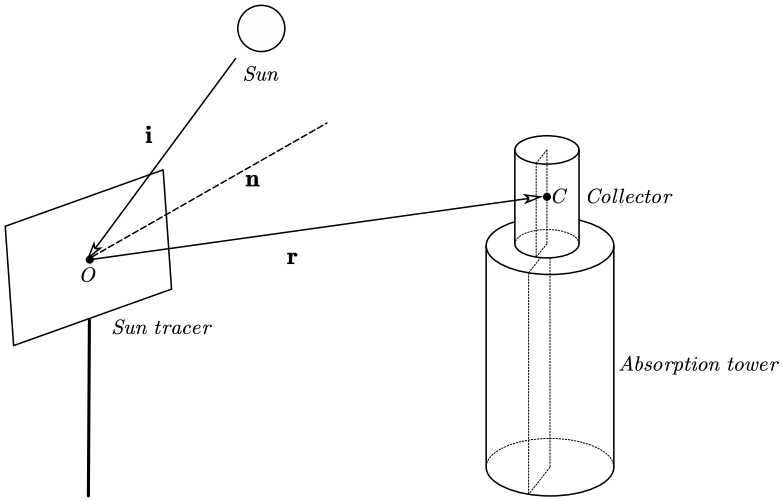

Figure 7. Schematic Diagram for Normal Vector Solution

In Figure 7, point O represents the center of the heliostat, point C is the center of the receiver, $\vec{i}$ is the vector direction of the incident solar rays, $\vec{r}$ is the vector direction of the reflected solar rays, and $\vec{n}$ is the normal vector of the heliostat surface. According to the law of reflection, the angle of reflection is equal to the angle of incidence, i.e., $\theta_i = \theta_r$. It is posited that $\vec{i}_{||}$ is the parallel vector to $\vec{r}_{||}$, and $\vec{r}_{\perp}$ is the antiparallel vector to $\vec{i}_{\perp}$, leading to the following relationships:

$$\begin{cases} \vec{i}_{\perp} = -\left|\vec{i}_{\perp}\right|\vec{n} = \left(\vec{i}\cdot\vec{n}\right)\vec{n} \\ \vec{i}_{|} = \vec{i} - \vec{i}_{\perp} \end{cases} \tag{3}$$

$$\Rightarrow \vec{r} = \vec{r}_{|} + \vec{r}_{\perp} = \vec{i}_{|} - \vec{i\perp} = \vec{i} - 2\vec{i}_{\perp} = \vec{i} - 2\left(\vec{i}\cdot\vec{n}\right)\vec{n}$$

The article then derives the equation of the reflected light ray as follows:

$$\frac{x - P(x)}{r(x)} = \frac{y - P(y)}{r(y)} = \frac{z - P(z)}{r(z)} \tag{4}$$

3. Model Solution

3.1. Atmospheric Transmittance

The expression for the atmospheric transmittance η_{at} is provided:

$$\eta_{at} = 0.99321 - 0.0001176 d_{\mathrm{HR}} + 1.97 \times 10^{-8} \times d_{\mathrm{HR}}^2 \quad (d_{\mathrm{HR}} \leq 1000) \tag{5}$$

which includes the variable d_{HR}, representing the distance from the center of the mirror surface to the center of the receiver [2-5].

3.2. Mirror Reflectivity

Given that the reflectivity η_{ref} of the mirror surface is a constant, typical values range between 0.85 and 0.95. For simplification in calculations, this study assumes a uniform reflectivity of 0.92 for all mirror surfaces.

3.3. Heliostat Field Thermal Power Output

$$E_{\mathrm{field}} = \mathrm{DNI} \cdot \sum_{i}^{N} A_i \eta_i \tag{6}$$

Where DNI represents the Direct Normal Irradiance, N is the total number of heliostats, A_i is the light-collecting area of the ith heliostat, and η_i is the optical efficiency of the i_{th} heliostat [6-8].

3.4. Comprehensive Problem Solving

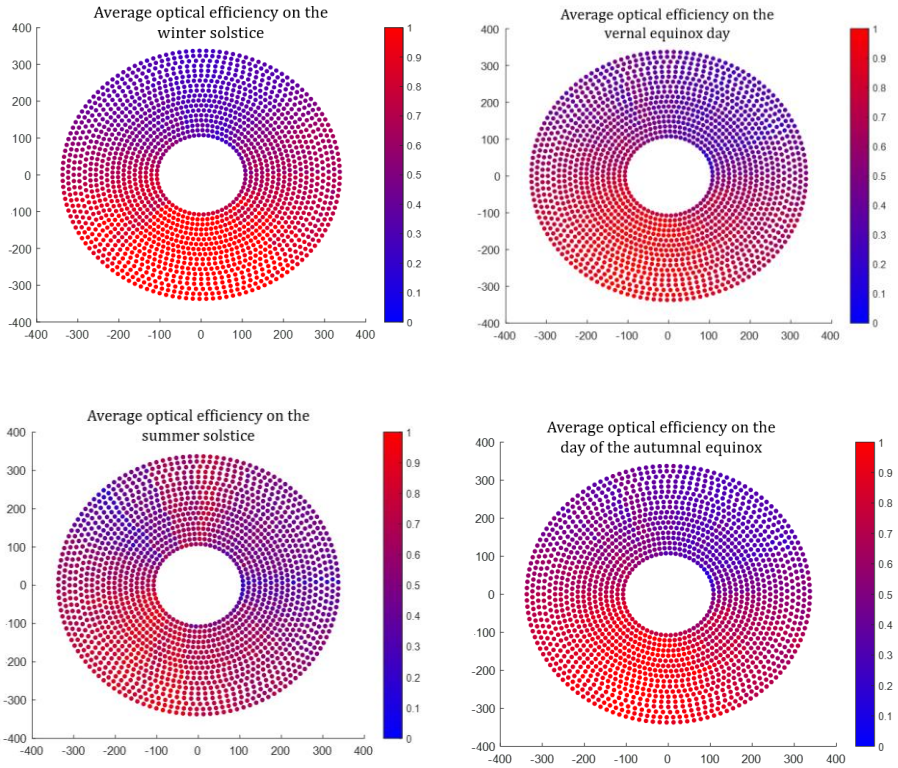

Figure 8. Diagram of Average Optical Efficiency for Various Solar Terms

Figure 8 represents the average optical efficiency of the heliostat field for four specific solar terms. This figure visually displays the average optical efficiency of each panel, with redder colors indicating higher efficiency and bluer colors indicating lower efficiency [9-11]. It provides an intuitive overview of the overall optical efficiency across the heliostat field (Table 1 and Table 2).

Table 1. Average Optical Efficiency and Power Output on the 21st of Each Month

Date	Average Optical Efficiency	Average Cosine Efficiency	Average Shadow-Blocking Efficiency	Average Stage Efficiency	Average Thermal Power Output per Unit Mirror Area (kW/m^2)
Jan 21	0.7199	0.9515	0.8933	0.5448	0.4765
Feb 21	0.7404	0.8963	0.8918	0.5233	0.4947
Mar 21	0.7611	0.8313	0.9021	0.5012	0.4994
Apr 21	0.7793	0.7826	0.9074	0.4827	0.4972
May 21	0.7893	0.7689	0.905	0.4788	0.5005
Jun 21	0.7924	0.7689	0.9049	0.4812	0.5051
Jul 21	0.7892	0.769	0.9048	0.4788	0.5004
Aug 21	0.7786	0.7843	0.9075	0.4835	0.4975
Sep 21	0.7601	0.8349	0.9011	0.5023	0.4994
Oct 21	0.7378	0.9036	0.891	0.5262	0.4934
Nov 21	0.7182	0.9578	0.8928	0.5471	0.4745
Dec 21	0.7111	0.9712	0.8927	0.5509	0.4598

Table 2. Annual Average Optical Efficiency and Power Output Table

Optical Efficiency	Annual Average Cosine Efficiency	Annual Average Shadow-Blocking Efficiency	Annual Average Truncation Efficiency	Annual Average Thermal Power Output (MW)	Power Output per Unit Mirror Area (kW/m^2)
0.5084	0.7565	0.8517	0.8996	30.879	0.4915

4. Conclusions

The study finds that the average power output of the heliostat field is highest during the summer solstice, reaching 0.5051 kW/m^2. Due to its location in the Northern Hemisphere, heliostats in the southern part of the field exhibit higher efficiency. The Monte Carlo algorithm is central to this research, offering benefits like strong universality, programming friendliness, and high adaptability, especially useful in calculating shadow blocking and truncation efficiency. However, it has the drawback of requiring large sample sizes to reduce error, leading to extensive computational demands. Despite these challenges, a balance has been struck to ensure the model's feasibility and accuracy. Future research will focus on potential improvements, especially in reducing computational requirements to leverage the inherent advantages of randomized algorithms for higher efficiency and accuracy in the study.

References

[1] ZHANG Ping, XI Zhengwen, HUA Wenhan, et al. Calculation method of optical efficiency of solar tower photothermal mirror field [J]. Technology and Market, 2021, 28(06): 5-8.)

[2] O. Farges, J.J. Bezian, M. El Hafi, Global optimization of solar power tower systems using a Monte Carlo algorithm: Application to a redesign of the PS10 solar thermal power plant [J], Renewable Energy, 2018, 119: 345-353.

[3] Du Yuhang, Liu Xiangmin, Wang Xingping, Jiang Zhihao. Analysis on the influence of different focusing strategies of heliostat in tower solar thermal power station [J]. Journal of Power Engineering, 2020, (40(05)).

[4] ZHANG Hong, KANG Tong. Model construction and solution of solar shadow positioning [J]. Journal of Communication University of China(Natural Science Edition), 2019, (26(06)).

[5] LIU Jianxing. Modeling and simulation of optical efficiency of tower solar thermal power station and optimal arrangement of heliostat mirror field [D]. Lanzhou Jiaotong University, 2022.

[6] Chao L, Rongrong Z. A novel solar tower assisted pulverized coal power system considering solar energy cascade utilization: Performance analysis and multi-objective optimization [J]. Renewable Energy, 2024, 222119891.

[7] Jing N, Hao S, Jing J, et al. Square solar updraft tower coupled phase change material: An experiment [J]. Applied Thermal Engineering, 2024, 240122229.

[8] Tao H, K. A A, Yongfeng J, et al. Integration of vanadium-chlorine thermochemical cycle with a nano-particle aided solar power tower for power and hydrogen cogeneration [J]. International Journal of Hydrogen Energy, 2024, 52(PC): 580-593.

[9] Lv Caixia. Effect of heliostat parameters on the performance of tower solar concentrating system [J]. Engineering Science and Technology II. Series, 2023, (42(05)).

[10] WANG Haoxuan, WANG Yiming. Sun shadow localization based on MATLAB software [J]. Science and Technology Innovation, 2019, ((13)).

[11] HUANG Yaqun, LI Xingyu, REN Yingying, TIAN Run, ZHANG Huaixiong. Experimental Science and Technology, 2018, (16(02)).